

Metal Enrichment in the Early Galactic Halo

Chisato IKUTA and Nobuo ARIMOTO

Institute of Astronomy, School of Science, University of Tokyo, Mitaka, Tokyo 181-8588, JAPAN

E-mail(CI): ikuta@mtk.ioa.s.u-tokyo.ac.jp

(Received 1998 November 02; accepted 1999 May 17)

Abstract

An early history of metal enrichment in the Galactic halo is studied. We investigate chemical inhomogeneity by using a stochastic chemical evolution model. The model confronts with metallicity distribution function of long-lived halo stars which is found to be a clue to obtain the best model prescriptions. We find that the star formation in the halo virtually terminated by ~ 1 Gyr and that the halo has never been chemically homogeneous in its star formation history. This conclusion does not depend whether mass loss from the halo is taken into account or not. Observed ratios of α -elements with respect to iron do not show scatters on a $[\alpha/\text{Fe}]-[\text{Fe}/\text{H}]$ plane, but this does not imply that interstellar matter in the halo was homogeneous because a chemical evolution path on this diagram is degenerate in the star formation rate. On the other hand, apparent spread of $[\text{Sr}/\text{Fe}]$ ratio among metal-poor halo stars does not reflect an inhomogeneous metal enrichment, instead it is due to a sharp increase in a production rate of strontium that is probably synthesised in slightly less massive stars than progenitor of iron-producing SN II.

1. Introduction

At very beginning of enrichment history of the Galactic halo, interstellar medium (ISM) was certainly chemically inhomogeneous, because star forming regions at that time were locally confined and stellar ejecta did not spread uniformly throughout the halo. Only a limited number of Type II supernovae (SN II) exploded and a mean spatial separation of SN II was much larger than a typical radius of single supernova remnant (Audouze & Silk 1995). Thus, the ISM was enriched locally. A trace of such inhomogeneous ISM should be frozen in extremely metal-deficient stars which we observe today (e.g. McWilliam 1997).

Nevertheless, no clear evidence which suggests that the halo was inhomogeneous in the past has so far been found. McWilliam et al. (1995), Audouze & Silk (1995), and McWilliam (1997) claimed that large scatters of *heavy metal* abundances (e.g., Sr, Y, Zr, Ba, and Eu) of extremely metal-poor halo stars (Beers, Preston, & Shectman 1992; McWilliam et al. 1995; Ryan, Norris, & Beers 1996) imply that the early halo was inhomogeneous. However, these scatters may simply reflect various lifetime of stars producing heavy metals, whose origins are poorly understood yet. The abundance of each heavy metal should sharply rise at a time when bulk of massive stars that produce it start to explode. Thus stars formed during such epoch should show a large scatter in relative abundance of heavy metals with respect to iron while they have nearly identical iron content. Therefore large scatters of heavy metals at certain values of $[\text{Fe}/\text{H}]$ do not necessarily imply an inhomogeneous ISM in an

early halo.

On the other hand, even if relative abundance of α -elements (e.g., O, Mg, Si, Ca, etc) with respect to iron do show little scatter at any value of $[\text{Fe}/\text{H}]$, it does not necessarily mean that an early halo was homogeneous. Even if a star formation history of each region in the halo is different from each other, evolutionary paths on the $[\alpha/\text{Fe}]-[\text{Fe}/\text{H}]$ plane should be nearly identical in an early evolutionary stage during which SN II were dominant sources of nuclear enrichment. The evolutionary path depends on a star formation rate (SFR) very weak.

Although little is known about an early halo, there seems to be a clear evidence for the inhomogeneous ISM in a solar neighbourhood disc; long-lived dwarfs (e.g., Edvardsson et al 1993) show a spread of ~ 1 dex in iron abundance along poorly defined age-metallicity relation. By relaxing a usual assumption of well mixing, Copi (1997) estimated chemical evolution of the solar neighbourhood in a Monte Carlo fashion. The solar neighbourhood is modeled by 1000 independent regions. The evolutionary history of one particular region is determined randomly based on the SFR and the initial mass function (IMF). Although he successfully reproduced the observed spreads of elemental ratios, he failed to explain the scatter appeared in the age-metallicity relation. Bateman & Larson (1993) suggested that random walk processes of atomic and molecular gas clouds are dominant mixing mechanisms of iron in the present day solar neighbourhood disc. Wielen, Fuchs, & Dettbarn (1996) suggested that stellar orbital diffusion in combination with radial abundance gradients can induce inhomogeneity in the ISM. However, van den Hoek & de Jong (1997) showed

that the stellar orbital diffusion does not explain the abundance variation sufficiently. They suggested instead that a sequential star formation and an infall of metal-deficient gas play an important role in preventing the ISM from being mixed. Wilmes & Köppen (1995) studied chemical evolution of isolated individual ISM parcels and showed that mixing is inefficient in the galactic disc. Pilyugin (1996) suggested that major galaxy mergers form multiple stellar populations of different metallicities in the disc. While these mechanisms can well explain the scatters along the age-metallicity relation, one should also keep in mind that stellar abundances may not reflect abundances of ISM from which stars formed, because chemical condensation processes such as grain formation in circumstellar envelope (e.g. Henning & Gürlér 1986) and/or thermal diffusion in stellar atmosphere (e.g. Bahcall & Pinsonneault 1996) might work efficiently.

If the early Galactic halo was chemically inhomogeneous, the metallicity spread should appear among halo stars of the same age. Unfortunately, the present day stellar isochrone fitting cannot distinguish age of stars born in a young halo. Therefore, it is not clear at all if the metallicity spread exists among coeval halo stars. Instead, we show in this paper that one can use an observed cumulative metallicity distribution function of halo stars to constrain stochastic chemical evolution models for an early halo and indicate that the Galactic halo has never been chemically homogeneous in its history.

In section 2, we give prescriptions for our stochastic chemical evolution models, and in section 3 we describe behaviours of theoretical metallicity distributions. We confront model results with observational data in section 4 and give discussions and conclusions in section 5 and 6, respectively.

2. Model

2.1. Outline

We have built up stochastic chemical evolution models for the Galactic halo. We assume that the halo is spheroidal and that the gas of primordial abundance distributed uniformly at the beginning. We divide the halo into many cubic blocks having a volume of $l_b^3 = 4\pi R_m^3/3$, where R_m is a radius of supershell caused by SN II that contributed dominantly to an early stage of chemical evolution. Progenitor of SN II are massive stars which tend to form in star clusters and associations (Blaauw 1964; Humphreys 1978; Heiles 1987). Supernova remnants in OB associations and star clusters are suggested to produce surrounding shell structures, or supershells (e.g., Tenorio-Tangle & Bodenheimer 1988). Cash et al. (1980) predicted that the supershell is produced after a series of SN II explosions. A radius of supershell can roughly be given as a maximum size of the area enriched by syn-

thesised heavy elements. Thus we assume that a volume of the block is equal to that of the supershell. The ISM in the supershell should be well-mixed, because stellar winds and SN II explosions induce the Rayleigh-Taylor and the Kelvin-Helmholtz instabilities (Tenorio-Tagle & Bodenheimer 1988; Allen & Burton 1993). The time scale of mixing is less than 0.0015 Gyr in a case of ionised gas (Roy & Kunth 1995), thus is much shorter than a typical lifetime (~ 0.01 Gyr) of the OB association. Once the mixing took place, the ISM in a block uniformly enriched by newly synthesised elements. Therefore, individual regions can be regarded as independent one-zones and a standard chemical evolution model can be applied for each of them.

Before an onset of star formation, all blocks have identical physical properties. We therefore follow chemical enrichment histories of 1000 neighbouring blocks instead of the all. Unless a number of blocks considered is too small, the resulting behaviour of each block is sufficiently stable. By simulating stochastic chemical evolution for 1000 blocks simultaneously, we calculate time variations of abundances in individual blocks and study chemical inhomogeneity in the halo.

2.2. Block Size

In an analogy to an expansion of single supernova, we roughly estimate a radius of the supershell as follows, although more detailed models for the supershells were published by several authors (Bruhweiler et al. 1980; McCray & Kafatos 1987; Mac Low & McCray 1988). Cioffi, McKee, & Bertschinger (1988) gave an analytical estimate for a radius r_m of a supernova remnant (SNR):

$$r_m = 69 E_{51}^{0.32} n^{-0.41} v_{10}^{-0.43} (Z/Z_\odot)^{-0.05} \text{ pc}, \quad (1)$$

where E_{51} is an initial kinetic energy of the SNR in units of 10^{51} erg, n is the number density of surrounding ISM, v_{10} is an ISM velocity dispersion in units of 10 km s^{-1} , and Z/Z_\odot is the ISM heavy element abundance. We calculate a radius R_m of the supershell by replacing E_{51} with $n_{\text{II}} E_{51}$, where n_{II} is the number of SN II in an OB association. Hereafter we adopt $E_{51} = 1$ (Shigeyama, Nomoto, & Hashimoto 1988). We assume that the velocity dispersion of ISM is equal to the sound velocity, and adopt $v \simeq 10 \text{ km s}^{-1}$ or $v_{10} \simeq 1$, since the temperature should be near 10^4 K (Hoyle 1953; Silk 1977) in the initial halo. Since we are interested in chemical evolution in the halo, we fix $Z/Z_\odot = 0.06$ which corresponds to $[\text{O}/\text{Fe}] \simeq 0.4$ (Barbuy 1988; Nissen et al. 1994) and $[\text{Fe}/\text{H}] = -1.6$; i.e., a peak iron abundance of the metallicity distribution function obtained for long-lived stars in the halo (Laird et al. 1988).

Stars having $M > 8M_\odot$, corresponding to main-sequence spectral type B3, eventually become SN II. The number of supernovae n_{II} is the number of such stars

per OB association. We adopt $n_{\text{II}} = 40$ according to Heiles (1987) who derived the average number of stars with $M > 8M_{\odot}$ per clusters from actual counting of O stars in clusters in the solar neighbourhood together with the IMF derived from clusters in the solar vicinity. The number Heiles (1987) got was ~ 28 , which was then corrected for runaway O stars that will deposit energy within the supershell. Significant deviations from the average value of n_{II} are apparently rare although n_{II} may cover a wide range of values (Tenorio-Tangle & Bodenheimer 1988).

The number density of the ISM is given as $n = M_{\text{h}}/(\mu m_{\text{H}} V_{\text{h}})$, where m_{H} is the proton mass, M_{h} is the mass, $V_{\text{h}} = \frac{4}{3}\pi R_{\text{h}}^3$ is the halo volume, and $\mu = 1.3$ is a mean molecular weight corresponding to the primordial compositions.

Saito (1979) derived an empirical relation between the binding energy Ω_{G} and the mass M_{G} by analysing surface brightness distributions and line-of-sight velocity dispersions of spheroidal systems:

$$\Omega_{\text{G}} = 1.66 \times 10^{60} \left[\frac{M_{\text{G}}}{10^{12} M_{\odot}} \right]^{1.45} \text{ erg.} \quad (2)$$

Under the assumption of spherical geometry, the radius $R(M_{\text{G}})$ of a galaxy is given as

$$R(M_{\text{G}}) = 26.1 \left[\frac{M_{\text{G}}}{10^{12} M_{\odot}} \right]^{0.55} \text{ kpc.} \quad (3)$$

We assume that the early Galactic halo follows the same mass-radius relation given by equation (3). The virial theorem tells that a system with initially no kinetic energy attains virial equilibrium by reducing a radius to half the initial value. Since we study chemical evolution at the very beginning, the radius of halo R_{h} should be taken as $2R(M_{\text{h}})$.

If we assume the halo was $M_{\text{h}} = 4 \cdot 10^{11} M_{\odot}$ (Fich & Tremaine 1991), then we obtain $R_{\text{h}} = 2R(M_{\text{h}}) = 31.5 \text{ kpc}$, and $n = 0.1 \text{ cm}^{-3}$. According to equation (1), the supershell radius R_{m} depends weakly on n . Since the amount of gas condensed into stars in the early stage of halo evolution is at most 25 percent, R_{m} changes only by 12 percent. We therefore assume n constant in time. Putting $n_{\text{II}} E_{51} = 40$, $n = 0.1 \text{ cm}^{-3}$, $v_{10} \simeq 1$, and $Z/Z_{\odot} = 0.06$ into equation (1), we obtain $R_{\text{m}} \sim 660 \text{ pc}$ and $l_{\text{b}} \equiv (4\pi R_{\text{m}}^3/3)^{1/3} = 1 \text{ kpc}$ for our standard model.

A time t_{m} when a SNR merges with the surrounding ISM is given by (Cioffi et al. 1988),

$$t_{\text{m}} = 2 \cdot 10^6 E_{51}^{0.32} n^{-0.37} v_{10}^{-1.43} (Z/Z_{\odot})^{-0.05} \text{ yr,} \quad (4)$$

and a cooling time t_{c} inside a SNR (Cox 1972) as,

$$t_{\text{c}} = 5.7 \cdot 10^4 E_{51}^{4/17} n^{-9/17} \text{ yr.} \quad (5)$$

A lifetime of supershell T_{m} and a cooling time T_{c} inside the supershell can be derived by replacing E_{51} in

equations (4) and (5) with $n_{\text{II}} E_{51}$, respectively. Assuming the same parameters discussed above, we obtain $T_{\text{m}} \simeq 1.7 \cdot 10^{-2} \text{ Gyr}$ and $T_{\text{c}} \simeq 4.6 \cdot 10^{-4} \text{ Gyr}$. We note that T_{m} is much longer than T_{c} .

2.3. Star Formation Probability

Considering an idealised situation that the OB associations distribute uniformly in the halo, we assume that a star formation probability $P_{\text{SF}}(t)$ in a block for a time interval t and $t + \Delta t$ is given as,

$$\begin{aligned} P_{\text{SF}}(t) &= \frac{l_{\text{b}}^3}{V_{\text{h}}} \frac{1}{n_{\text{II}}} \int_t^{t+\Delta t} N_{\text{II}}(t') dt' \\ &= \frac{3}{4\pi} \left(\frac{l_{\text{b}}}{R_{\text{h}}} \right)^3 \frac{1}{n_{\text{II}}} \int_t^{t+\Delta t} N_{\text{II}}(t') dt', \end{aligned} \quad (6)$$

where $N_{\text{II}}(t)$ is the total number of progenitor of SN II in the halo and is given as,

$$N_{\text{II}}(t) = M_{\text{h}} C(t) f_{\text{II}}, \quad (7)$$

where $C(t)$ is the SFR per unit mass and f_{II} is the number fraction of SN II defined as,

$$f_{\text{II}} = \int_{m_{\text{II}}}^{m_{\text{u}}} \phi(m) m^{-1} dm, \quad (8)$$

with $m_{\text{l}} = 0.1 M_{\odot}$, $m_{\text{u}} = 50 M_{\odot}$, and $m_{\text{II}} = 10 M_{\odot}$ as the lower and the upper mass limits, and the lower SN II mass limit, respectively. The IMF adopted here has mass spectrum independent of time:

$$\phi(m) = \frac{(x-1) m_{\text{l}}^{x-1}}{1 - (m_{\text{l}}/m_{\text{u}})^{x-1}} m^{-x}, \quad (m_{\text{l}} \leq m \leq m_{\text{u}}). \quad (9)$$

We adopt the Salpeter IMF (Salpeter 1955) which has a slope $x = 1.35$ in this definition. For $C(t)$, we adopt the Schmidt law (Schmidt 1959):

$$C(t) = \omega^{-1} G(t)^p \quad (p = 1), \quad (10)$$

where ω and $G(t)$ are time scale of star formation and a gas fraction in the halo, respectively. $P_{\text{SF}}(t)$ is thus finally given as:

$$\begin{aligned} P_{\text{SF}}(t) &= \frac{3}{4\pi} \left(\frac{l_{\text{b}}}{R_{\text{h}}} \right)^3 n_{\text{II}}^{-1} f_{\text{II}} M_{\text{h}} \omega^{-1} G(t)^p \Delta t \\ &\quad (p = 1). \end{aligned} \quad (11)$$

We adopt $m_{\text{II}} = 10 M_{\odot}$ in equation (8), which is slightly larger than $m_{\text{II}} = 8 M_{\odot}$ which Heiles (1987) adopted. Thus, equation (11) may underestimate $P_{\text{SF}}(t)$. A difference corresponding to the adopted m_{II} is ~ 12 percent. However, an exact value of m_{II} is still uncertain and, therefore, we adopt $m_{\text{II}} = 10 M_{\odot}$ for our standard model and change it later as a free parameter.

2.4. Chemical Evolution

For the blocks in which stars are born (hereafter the star forming blocks), we apply a chemical evolution model developed by Pagel & Tautvaišienė (1995; hereafter PT95). We adopt the iron as a tracer of chemical evolution. In PT95, the iron abundance is calculated by using an instantaneous recycling approximation and a delayed production approximation which assumes that the iron is additionally produced by Type Ia supernovae (SNIa) after a fixed time lag τ_1 . We assume that the SFR $c(t)$ in a block is proportional to the gas fraction $g(t)$. The iron abundance $Z_{\text{Fe}}(t)$ is given by,

$$\frac{d(gZ_{\text{Fe}})}{dt} = \begin{cases} -Z_{\text{Fe}}(t)c(t) + p_0c(t), & (t < \tau_1), \\ -Z_{\text{Fe}}(t)c(t) + p_0c(t) + p_1c(t - \tau_1), & (t \geq \tau_1), \end{cases} \quad (12)$$

where p_0 and p_1 are yields of iron corresponding to the instantaneous recycling approximation and the delayed production approximation, respectively. The first term on the right hand side (r.h.s.) represents the net amount of iron locked into newly formed stars. The second and the third terms are corresponding to the instantaneous recycling approximation and the delayed production approximation, respectively. We adopt $p_0 = 0.28$, $p_1 = 0.42$, and $\tau_1 = 1.3$ Gyr according to PT95. Since the theoretical yields of the iron are uncertain due to difficulties in modeling the explosion mechanism (Timmes, Woosley, & Weaver 1995), we use the yields of PT95 which are calibrated empirically.

The SFR in each block $c(t)$ is determined by an assumed number of SN II exploded in a block during a time interval t and $t + \Delta t$:

$$\int_t^{t+\Delta t} m_b f_{\text{II}} c(t') dt' = n_{\text{II}}, \quad (13)$$

where $m_b = M_h l_b^3 / V_h \simeq 3 \cdot 10^6 M_\odot$ is the initial gas mass of each block.

2.5. Standard Models

Table 1 gives a list of parameters adopted for our standard models S1, S2, and S3. In model S1 we assume that the OB associations are formed randomly at every $\Delta t \sim \frac{1}{3} T_m = 0.006$ Gyr. In model S2 we introduce an effect of periodic mixing due to the turbulent diffusion. A particle with a sound velocity $v = 10 \text{ km s}^{-1}$ would across a block of size $l_b = 1$ kpc in $T_d = 0.1$ Gyr. Thus, we assume in this model that every 0.1 Gyr the turbulent diffusion mixes the 27 blocks surrounding the star forming block periodically.

The supershell structures are often mentioned as a trigger of massive star formation. The evidences have been discussed by many authors (Blaauw 1964; Elmegreen & Lada 1977; Lada, Blitz, and Elmegreen 1979; Elmegreen 1982; 1985a, b). If OB associations form in this way, they should be born only in the surrounding area of the

Table 1. Parameters of standard model.

M_h	$4 \cdot 10^{11} M_\odot$	mass of the halo
R_h	31.5 kpc	radius of the halo
ω	5 Gyr	time scale of star formation in the halo
l_b	1 kpc	size of a block
v_{10}	1	velocity dispersion of ISM in units of 10 km s^{-1}
m_l	$0.1 M_\odot$	IMF lower mass limit
m_{II}	$10 M_\odot$	lower mass limit for SN II
n_{II}	40	number of SNe II in a block
Δt	$6 \cdot 10^6 \text{ yr}$	duration of star formation

star forming regions and chemical enrichment should be locally confined there. The effects of this stimulated star formation are studied in model S3. We first distribute OB associations randomly and then assign randomly a star forming block for the next generation among 27 blocks adjoining to each star forming block of the first generation and so on. In this way, the star formation propagates from one block to another.

The time step adopted for each simulation is 0.001 Gyr. Calculations are stopped at 1 Gyr, since our main interest is in early chemical evolution of the halo.

The time scale of star formation ω in the halo is quite uncertain. On the contrary, it is quite often assumed that ω in elliptical galaxies is of the order of free-fall time $t_{\text{ff}} = (3\pi/32G\bar{\rho})^{1/2}$ (Larson 1974). One could assume that ω in the halo is the same as that in giant ellipticals. However, mean stellar metallicities of giant ellipticals are nearly solar (Arimoto et al. 1997), while that of Galactic halo stars is $\sim 1/40$ solar (Ryan & Norris 1991; Carney et al. 1996). Both in giant ellipticals and in the galactic halo, Mg seems to be enhanced with respect to Fe by at least a factor of 2 (McWilliam et al 1995; Ryan et al 1996). This implies that star formation in both systems is characterised by the same IMF and that the star formation stopped before the onset of SNIa explosions (~ 1 Gyr). If this is the case, ω in the Galactic halo should be 40 times longer than that of giant ellipticals. Thus we obtain $\omega \simeq 40 t_{\text{ff}} \sim 6$ Gyr for our halo model with $M_h = 4 \cdot 10^{11} M_\odot$ and $R_h = 31.5$ kpc. Since $\omega \sim 6$ Gyr is very close to $\omega \sim 5$ Gyr derived for the solar neighbourhood disc (Arimoto, Yoshii, & Takahara 1992), we shall adopt $\omega = 5$ Gyr in our standard models. In other words, we adopt the same SFR for the Galactic halo and the solar neighbourhood disc.

3. Metallicity Distribution

Figure 1 shows the number fraction of blocks which at least once have experienced the chemical enrichment. Model S1 predicts that all the blocks have been enriched

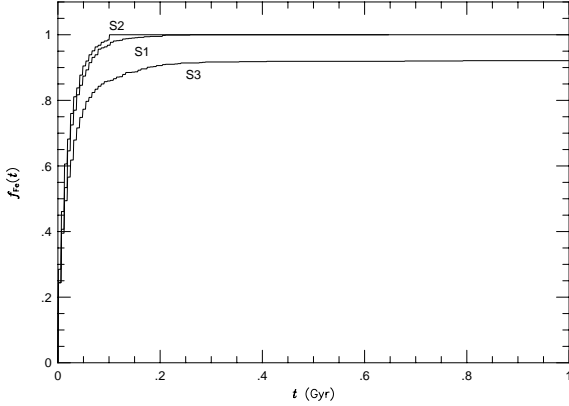


Fig. 1.. The evolution of the number fraction of blocks which at least once have experienced chemical enrichment in the standard models S1, S2, and S3.

before ~ 0.2 Gyr. In model S2, this happens earlier than model S1, because the iron spreads beyond the super-shells due to the turbulent diffusion, thus much wider area are enriched even if the SFRs are the same as in model S1. On the other hand, nearly 8% of the block in model S3 has never been enriched till 1 Gyr, this is because the stimulated star formation tends to localise the chemical enrichment.

Figures 2a and 2b show the evolution of mean and median iron abundances, respectively. Hereafter we discuss statistical properties except for the first 0.04 Gyr, during which the number of enriched blocks is too small to define the statistical properties. Figures 2a and 2b indicate that the median metallicities of models S1 and S2 are nearly the same as the mean metallicities. This suggests that the metallicity distributions of the two models have symmetric shapes. The median of model S3 is always higher than the mean, indicating that the metallicity distribution has a tail toward lower metallicity.

Figure 3 illustrates a frequency distribution of iron abundance of the 1000 blocks, $N([\text{Fe}/\text{H}])$, of model S1 at 0.01, 0.05, 0.1, 0.2, 0.5, and 1 Gyr. For an illustrating purpose, $N(-5 < [\text{Fe}/\text{H}] \leq -4.8)$ is artificially assigned for a fraction of metal-free blocks. Figure 3 shows that the metallicity distribution of model S1 has roughly 1.3 dex spread of the iron abundance, suggesting that the ISM in the halo was inhomogeneous till 1 Gyr.

Figure 4 gives the evolution of standard deviation of the metallicity distribution obtained by the standard models. In model S1, the standard deviation keeps nearly constant at $s(t) \simeq 0.24$ after ~ 0.2 Gyr, which corresponds to roughly 1.3 dex dispersion of the iron

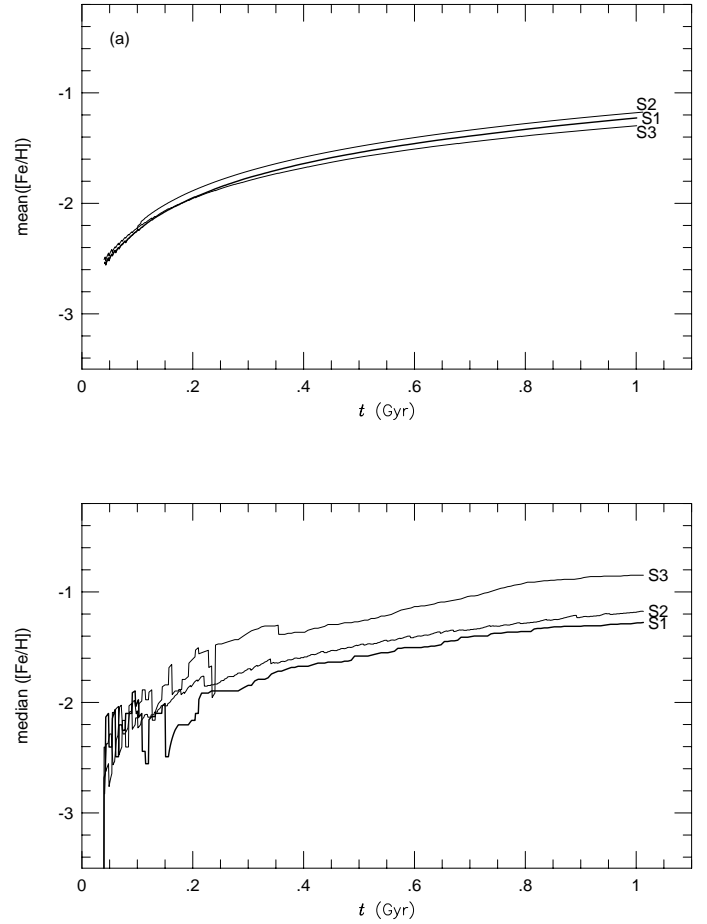


Fig. 2.. (a) The evolution of the mean iron abundance in the standard models S1, S2, and S3. (b) The same as figure 2(a), but for the median iron abundance.

abundance. Model S3 suggests much stronger abundance spread than model S1. The standard deviation of model S3 increases with time and exceeds 0.5 at 1 Gyr, which is roughly equivalent to 2 dex dispersion of the iron abundance among all the enriched blocks. On the other hand, the standard deviation of model S2 decreases quickly to nearly zero, showing that the ISM was homogeneous from the very beginning of its chemical evolution.

Now we focus on the shape of the metallicity distribution. Figures 5a and 5b illustrate the skewness and the kurtosis of the metallicity distributions of the standard models, respectively (e.g. Stuart & Ord 1987). The skewness characterises a degree of asymmetry of a distribution around its mean. It characterises only a shape of the dis-

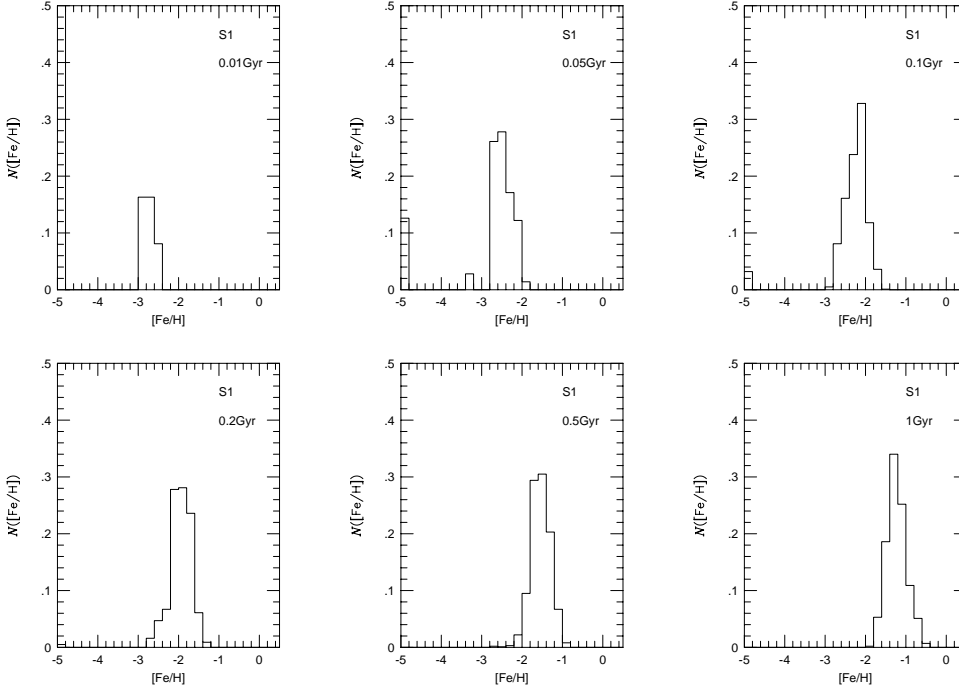


Fig. 3.. The frequency distribution of iron abundance of the 1000 blocks in model S1 at 0.01, 0.05, 0.1, 0.2, 0.5, and 1 Gyr.

tribution. The definition is

$$\text{Skew}(x_1, x_2, \dots, x_N) = \frac{1}{N} \sum_{i=1}^N \left(\frac{x_i - \bar{x}}{s} \right)^3, \quad (14)$$

where \bar{x} and s are the mean and the standard deviation of the measured value x_1, x_2, \dots, x_N . A positive value of skewness signifies a distribution with an asymmetric tail extending out towards larger x , while a negative value signifies a distribution whose tail extends out towards smaller x . The definition of the kurtosis is

$$\text{Kurt}(x_1, x_2, \dots, x_N) = \left\{ \frac{1}{N} \sum_{i=1}^N \left(\frac{x_i - \bar{x}}{s} \right)^4 \right\} - 3, \quad (15)$$

where the first term of r.h.s. becomes 3 for a Gaussian distribution. The kurtosis measures the relative peakedness or flatness of a distribution relative to the Gaussian distribution. The distribution with positive kurtosis has

the outline of the Matterhorn for example. The distribution with negative kurtosis is outlined of a lump of meat-loaf. Figure 5a gives the evolution of skewness of the standard models. The skewness of model S1 is nearly zero, which means a symmetric shape of the metallicity distribution. The skewness of model S2 behaves irregularly due to nearly null standard deviation. The skewness of model S3 is always negative and decreases as times goes on, showing a tail of the metallicity distribution extending toward lower metallicity at later stages. This is due to the localised chemical enrichment caused by the stimulated star formation. Figure 5b shows the evolution of kurtosis. The kurtosis of model S1 is nearly equal to zero, thus the metallicity distribution has a Gaussian like shape. On the contrary, the kurtosis of model S2 is very large. This model suggests the homogeneous ISM, since the kurtosis should be infinitely large if samples have the same value. In model S3, the kurtosis gradually increases up to ~ 2 , which means that the metallicity distribution

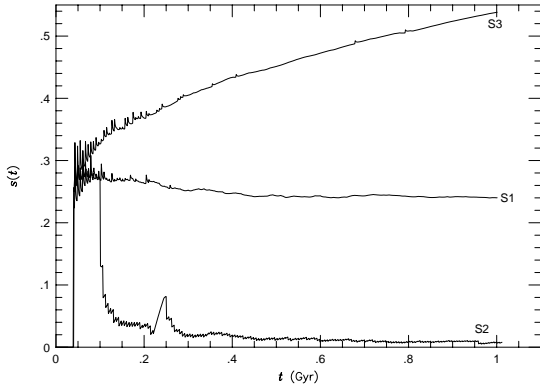


Fig. 4.. The evolution of standard deviation of metallicity distribution in the standard models S1, S2, and S3.

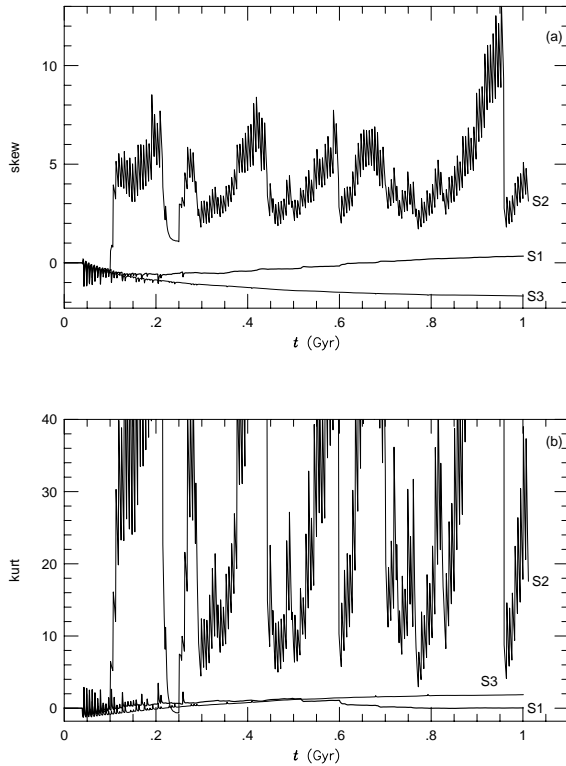


Fig. 5.. (a) The evolution of skewness of metallicity distribution of the standard models S1, S2 and S3. (b) The same as figure 5a, but for the kurtosis of metallicity distribution.

has a sharp peak. Thus the skewness and the kurtosis of model S3 indicate that the metallicity distribution has a peaked shape with a tail extending to the lower metallicity.

As a summary, only model S2 shows that the ISM was chemically homogeneous in the early halo, while both

models S1 and S3 show that the ISM in the halo was not well-mixed till at least 1 Gyr. Indeed, the scatters of the iron abundance are roughly 1.4 dex in model S1 and 2 dex in model S3, respectively. We have repeated the simulations several times and confirm that the model results show always the same tendencies.

4. Observational Constraints

Long-lived stars in the halo should keep the original metallicities of the ISM from which they formed. It is true that little observational information is available for constraining chemical evolution models of the halo, but we will show that a cumulative metallicity distribution function of the long-lived halo stars can potentially give a powerful clue to obtain the best model prescriptions.

4.1. Comparison with the Standard Models

Figures 6 and 7 present generalised metallicity distribution functions (GMDFs), $P([\text{Fe}/\text{H}])$, of the standard models S1 – S3 together with the empirical GMDFs of long-lived halo stars taken from Ryan & Norris (1991) and Carney et al. (1996). The definition of GMDF is given by Laird et al. (1988):

$$P(x) = \frac{1}{N\sigma\sqrt{2\pi}} \sum_{i=1}^N \exp \left[-\frac{(x - x_i)^2}{2\sigma^2} \right], \quad (16)$$

where σ reads as a typical error in the observed values x_1, x_2, \dots, x_N .

Quite often, the empirical metallicity distribution function is presented in the form of a histogram. However, Searle & Zinn (1978) suggested that the bins of a conventional histogram should be replaced by a continuous distribution function such as a Gaussian to obtain a better approximation to the actual abundance distribution function, since the binning distorts the data. Therefore, we convolve the observed histograms of stellar metallicity distribution to include the uncertainty of observational data properly (Laird et al 1988) and convolve the theoretical GMDFs by using equation (16) with $\sigma = 0.15$ (Ryan & Norris 1991; Carney et al. 1996). We note that the GMDFs of Ryan & Norris (1991) and Carney et al. (1996) are almost identical, except that the latter shows a small hump at $[\text{Fe}/\text{H}] \simeq -2.7$.

Figure 6 shows that model S1 gives good fits to the observed GMDFs at 0.5 Gyr and 1 Gyr. The star formation in the halo must have virtually stopped at around 0.5 Gyr, otherwise the resulting GMDF gives too high peak metallicity. This would happen if the gas escapes from the halo and accretes on to the bulge and disc dissipationally. A precise value of the epoch when the star formation terminated is of course model dependent. However, the

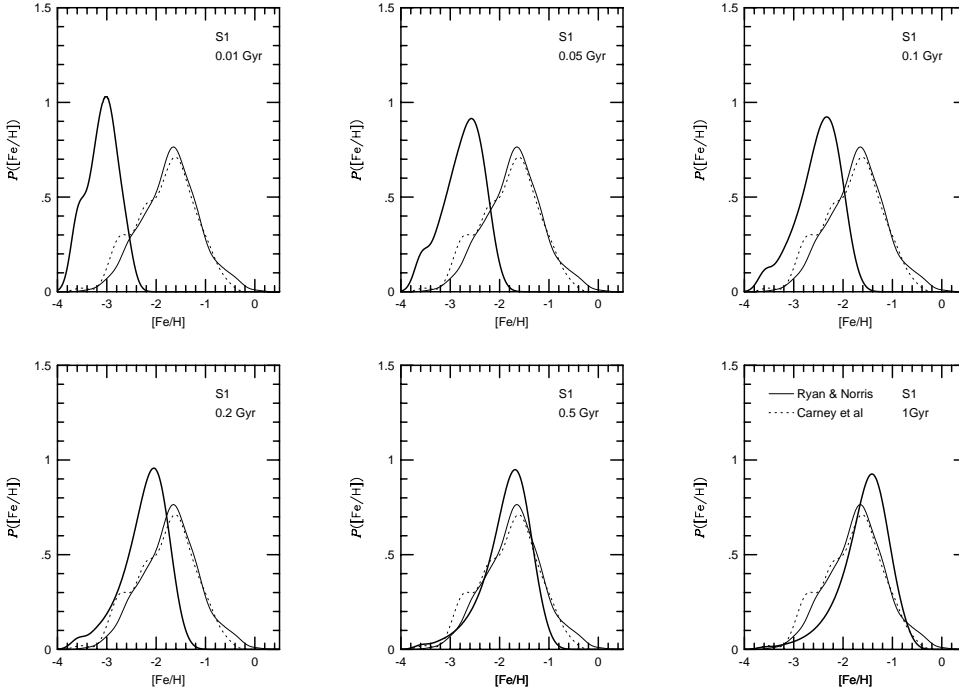


Fig. 6.. The generalised metallicity distribution functions (GMDFs) of model S1 at 0.01, 0.05, 0.1, 0.2, 0.5, and 1 Gyr (thick solid line). Thin solid and dotted lines illustrate the empirical halo GMDFs taken from Ryan & Norris (1991) and Carney et al. (1996), respectively.

GMDFs of halo stars strongly suggest that the star formation in the halo did not last longer than, say, 0.5–1 Gyr.

Upper and lower panels in figure 7 illustrate the GMDFs of models S2 and S3, respectively. Clearly, model S2 is inconsistent with the observations. Model S2 gives too sharp GMDFs to reproduce the observations. We have also studied several alternative cases in which we assume much longer time interval for the periodic turbulent mixing, much smaller size of the smoothed out area, and lower or higher probability of star formation, and have confirmed that these models give much sharper GMDFs than the empirical ones; thus inconsistent with the observations. On the contrary, the GMDF of model S3 is consistent with those observed. Equivalent models to model S3, but with higher or lower SFRs, are also calculated. These models predict similar inho-

mogeneous ISM enrichment. Their GMDFs are also consistent with the empirical ones at 0.1 Gyr (higher SFR) and 0.5 Gyr (lower SFR). The standard deviations of metallicity distribution function of these models increase with time, showing the same trends as those of model S3. Without additional informations, it is rather difficult to conclude which star formation mechanism, the spontaneous star formation (model S1) or the stimulated one (model S3), is responsible for the early enrichment of the Galactic halo.

To judge a goodness of the model fit to the empirical GMDFs, we have performed the χ^2 statistics. Let x_i and y_i be the theoretical and the observed $P([Fe/H]_i)$, respectively. Then, the χ^2 value is defined as,

$$\chi^2 = \sum_i \frac{(x_i - y_i)^2}{x_i + y_i}. \quad (17)$$

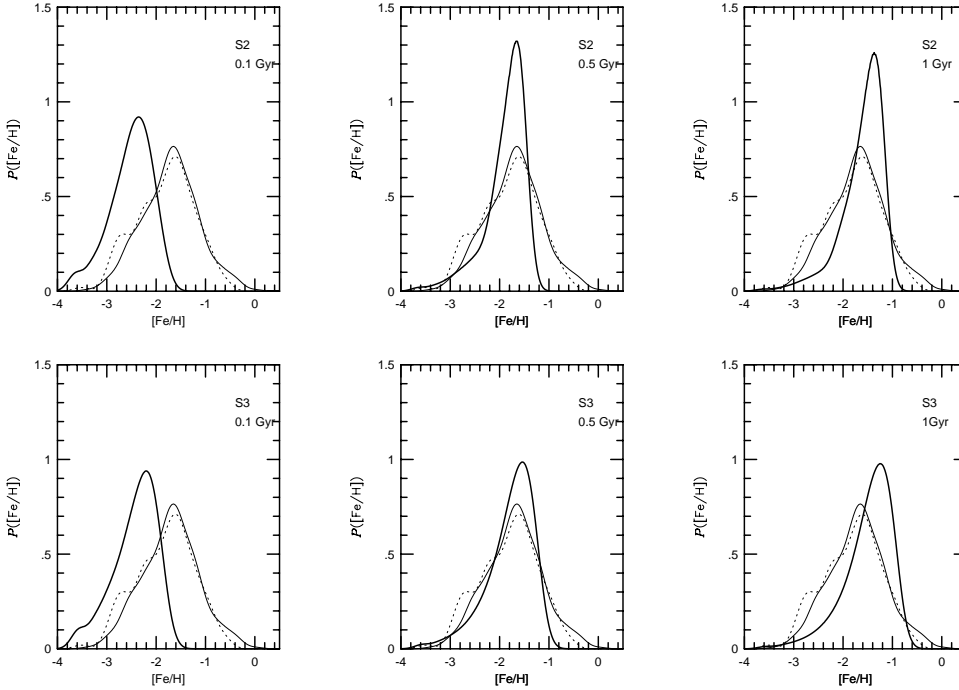


Fig. 7.. The GMDFs of model S2 (upper three panels) and model S3 (lower three panels) at 0.1, 0.5, and 1 Gyr. Thick solid lines show the theoretical GMDFs. Thin solid and dotted lines have the same meaning as in Fig. 6.

In columns (8)-(10) of table 2, we give the χ^2 values of the standard models at 0.1, 0.5, and 1 Gyr, respectively. The best fit is realised by model S1 at 0.5 Gyr, but model S1 at 1 Gyr and model S3 at 0.5 Gyr also give a reasonable fit.

In addition to the standard models, we show additional 7 models A - G to demonstrate the parameter dependence of our results. All the 7 models are equivalent to model S1, but with different parameters, i.e., these models assume spontaneous star formation and no turbulent mixing. The parameters of these 7 models are summarised in table 2. In this table, column (1) gives an identification of the model, columns (2) and (3) give the adopted values of l_b/R_h and $\omega^{-1}\Delta t$, respectively. Column (4) gives the parameter that is different from the standard models. Columns (5) - (7) indicate the standard deviation $s(t)$ at 0.1, 0.5, and 1 Gyr, respectively. The χ^2 values for the best fit epochs of the standard models are 11.01 (model S1) and 11.89 (model S3) at 0.5 Gyr. Therefore, we consider a good fit is realised if the model

gives the χ^2 less than 12 in columns (8) - (10).

In models A - C, we study how the evolution of $s(t)$ and χ^2 depend on l_b/R_h and $\omega^{-1}\Delta t$. Two cases of $l_b/R_h = 0.01$ and 0.03 are studied. For $\omega^{-1}\Delta t$, we consider three cases, i.e. $\omega^{-1}\Delta t = 0.6 \cdot 10^{-3}$, $1.2 \cdot 10^{-3}$, and $3 \cdot 10^{-3}$. The standard deviation of model A is always larger than that of model S1, which suggests that the ISM is always chemically inhomogeneous. In model B, higher SFRs lessen the differences of chemical enrichment among the blocks. The standard deviation of model B is nearly equal to 0.1 at 1 Gyr, predicting relatively well-mixed ISM with respect to model S1. However, the χ^2 of model B indicates that this model is inconsistent with the observations. In model C, given smaller l_b/R_h , the best fit epoch to the observations comes earlier than model S1. The gas in the star forming blocks of model C is converted into stars more efficiently than model S1, since equation (14) indicates that the SFR in a block is proportional to n_{II}/m_b , i.e., $(l_b/R_h)^{-3}$. In model D, we reduce the number of SN II progenitor in a single OB association and assume

Table 2. Models and results.

Model	l_b/R_h	$\omega^{-1}\Delta t$	$s(t)$			χ^2		
			0.1	0.5	1	0.1	0.5	1
S1	0.03	1.2	0.27	0.24	0.24	75.11	11.01	11.85
S2	0.03	1.2	0.27	0.01	0.01	76.82	26.78	22.63
S3	0.03	1.2	0.33	0.45	0.54	68.16	11.89	20.36
A	0.03	0.6	0.34	0.34	0.29	53.52	4.68	15.82
B	0.03	3	0.18	0.10	0.10	95.12	24.40	16.79
C	0.01	1.2	0.32	0.44	0.42	9.25	11.68	19.73
D	0.03	1.2	$n_{\text{II}} = 20$	0.15	0.11	92.31	21.39	17.19
E	0.03	1.2	$m_{\text{II}} = 8M_\odot$	0.24	0.16	83.33	16.70	14.02
F	0.03	1.2	$m_l = 0.05M_\odot$	0.30	0.33	62.80	6.19	11.77
G	0.03	1.2	$M_h = 2 \cdot 10^{11}M_\odot$	0.30	0.42	49.38	4.00	13.06

Model S2 assumes propagation of star formation. Model S3 assumes the mixing of ISM by turbulent diffusion whose period is taken to be 10^8 yr. See text in detail.

$n_{\text{II}} = 20$ instead of 40 (Blaauw 1964). This increases the probability of star formation (see equation (11)) and homogenises the ISM quickly. The χ^2 of model D indicates poor fits to the observations. Model E assumes $m_{\text{II}} = 8M_\odot$. The number fraction of SN II progenitor in model E is increased and the SFR becomes twice of model S1. Thus, both the evolutionary behaviour of standard deviation and the χ^2 fits are very similar to those of model B. We can reject this model, since the χ^2 gives very poor fits. Models F and G assume $m_l = 0.05M_\odot$ and $M_h = 2 \cdot 10^{11}M_\odot$, respectively. Equation (11) indicates that the probability of star formation $P(t)$ in a block, namely the SFR in the halo, is proportional to the number fraction f_{II} of SN II progenitor and the mass of the halo. Thus in models F and G with the lower SFR in the halo, the standard deviation of metallicity distribution function becomes slightly larger than that of model S1. The χ^2 values of models F and G show that these models give a good fit to the observed GMDFs in the halo at 0.5 Gyr.

In summary, the different parameters change the SFR in the halo. If the SFR is low, the standard deviation of metallicity distribution becomes large, i.e. the ISM is inhomogeneous, and good fits to the observed GMDFs are resulted. While if the SFR in the halo is high, the standard deviation becomes small (well-mixed ISM) and the resulting GMDFs show poor fits to the observations, since stars born in the similarly enriched ISM dominate the cumulative metallicity distribution function at later phase. Thus the predicted GMDF becomes too narrow to be consistent with the observations.

4.2. Comparison with Mass-Loss Models

In previous sections, we assume that the halo was a closed system. Hartwick (1976) showed that a simple

model predicts too many metal-poor stars and is inconsistent with the cumulative distribution of the iron abundances for metal-poor ($[\text{Fe}/\text{H}] \leq -0.52$) globular clusters in the Galactic halo. He modified the simple model and proposed a model which allows for gas outflow from the halo. We therefore consider effects of mass loss from the halo in this subsection. The gas will eventually either escape to intergalactic space or to accrete onto the galactic plane.

Since the gas removal from the halo could be related to energy injection from hot OB stars and SN II (Hartwick 1976), we assume that the mass loss rate dD/dt is proportional to the SFR $C(t)$:

$$\frac{dD}{dt} = bC(t). \quad (18)$$

The mass loss rate b and the SFR are taken from Hartwick (1976), i.e., $b = 10$ and $\omega^{-1} = 0.3$, respectively. We assume the same gas outflow rate for all the blocks in the halo. In model ML1, the parameters are the same as those of model S1 except for b and ω^{-1} . We assume that OB associations are born randomly in space and do not consider the ISM mixing by turbulent diffusion. While in model ML2, we study the effects of turbulent mixing. We assume periodic ISM mixing, similarly to model S2. The period is taken as 0.1 Gyr, the same as that of model S2. Other prescriptions for model ML2 are same as those of model ML1.

Figures 8a and 8b show the evolution of mean iron abundance and that of standard deviation of the mass loss models, respectively. Figure 9 shows the theoretical GMDFs plotted with the observed GMDFs. These figures show that the GMDFs obtained by model ML1 agree with the observed GMDFs and the ISM is always inhomogeneous in this model. On the other hand, the

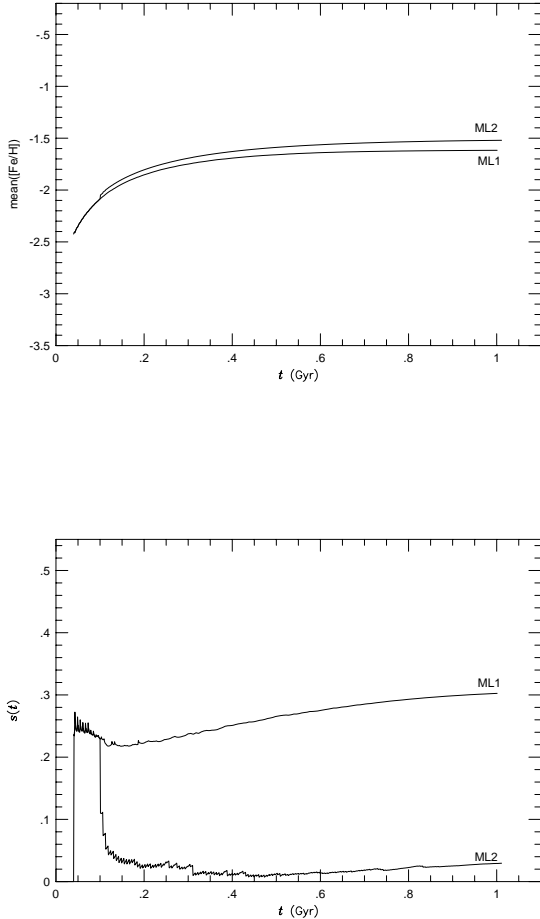


Fig. 8.. (a) The same as figure 2(a), but for mass loss models ML1 and ML2. The SFR $\omega^{-1} = 0.3$ and the mass-loss rate $b = 10$ are the same as those of Hartwick (1976). (b) The same as figure 4, but for mass-loss models ML1 and ML2.

GMDFs of model ML2 are too sharp and are inconsistent with the observations, because the ISM in this model is well-mixed. In model ML1, the best fit is achieved at an epoch later than model S1. In the case of one-zone model, a shift of the peak abundance can be explained by a decrease of effective yield caused by the mass-loss (Hartwick 1976; Pagel 1992). Although our model is not one-zone, the mass-loss gives a similar effect to the peak abundance of the cumulative metallicity distribution function.

The GMDFs obtained by assuming $b = 10$ and $\omega^{-1} = 0.2$ (the same SFR as that of model S1) also fit to the observed GMDFs and the best fit is realised at around 1 Gyr. The chemical enrichment in this model is also inhomogeneous. A model adopting $b = 5$ also gives consistent GMDFs with the observations, although the best

fit epoch appears earlier than model ML1 due to a larger effective yield. Gas outflow may occur in the vicinity of star forming regions, if major energy sources are massive stars. When we take this into account and consider a model in which gas is expelled only from the star forming blocks, we obtain the same results on a fitting goodness and inhomogeneity of the ISM as those obtained by models ML1 and ML2.

As a conclusion, whether or not mass loss is taken into account, the ISM in the halo at the beginning must be inhomogeneous.

5. Discussions

Observations show neither clear age-metallicity relation nor clear evidence for metallicity gradient in the halo. Because of these observational results, Galactic halo formation scenario favoured recently (e.g. Carney et al. 1996) is the one proposed by Searle & Zinn (1978), i.e. accretion of small proto-galactic fragments contributed to the halo population. However, in the poorly mixed halo, the age-metallicity relation and the metallicity gradient cannot be expected even if the Galaxy formed from one massive cloud. Thus it is not necessary to introduce the accretion of proto-galactic fragments to interpret the lack of the age-metallicity relation and the metallicity gradient in the halo.

The scatters observed in the relative abundances of neutron capture elements to the iron, particularly $[\text{Sr}/\text{Fe}]$, are often claimed as evidences for the inhomogeneous enrichment of the ISM in the halo at the very beginning. In figure 10, Sr abundances of halo stars taken from Gratton & Sneden (1988; 1994), Magain (1989), McWilliam et al. (1995), and Ryan et al. (1996) are plotted. The observations show that a majority of the metal-poor stars with $[\text{Fe}/\text{H}] \leq -2.5$ distribute at $-1.5 \leq [\text{Sr}/\text{Fe}] \leq 0.6$. The relative abundance of Sr tends to decrease clearly with an increase of the iron abundance.

We show two theoretical evolutionary paths of Sr on figure 10. The models are calculated by adopting the same parameters as those of models S1 (left path) and C (right path). The SFR of model S1 is nearly one tenth of model C. Co-existence of regions with different SFR is a view of the chemical evolution in the halo considered here. We have simplified the situation and assumed the same SFR in each block. However, different SFR in each star forming region is more realistic. These models are consistent with the observed behaviour of $[\text{Sr}/\text{Fe}]$ and the empirical metallicity distribution functions.

Following PT95 and Pagel & Tautvaišienė (1997; hereafter PT97), we calculate the chemical evolution of Sr:

$$\frac{d}{dt}(g_{\text{Sr}}) = -Z_{\text{Sr}}(t)c(t) + p_0c(t) + \sum_{i=1}^3 p_i c(t - \tau_i), \quad (19)$$

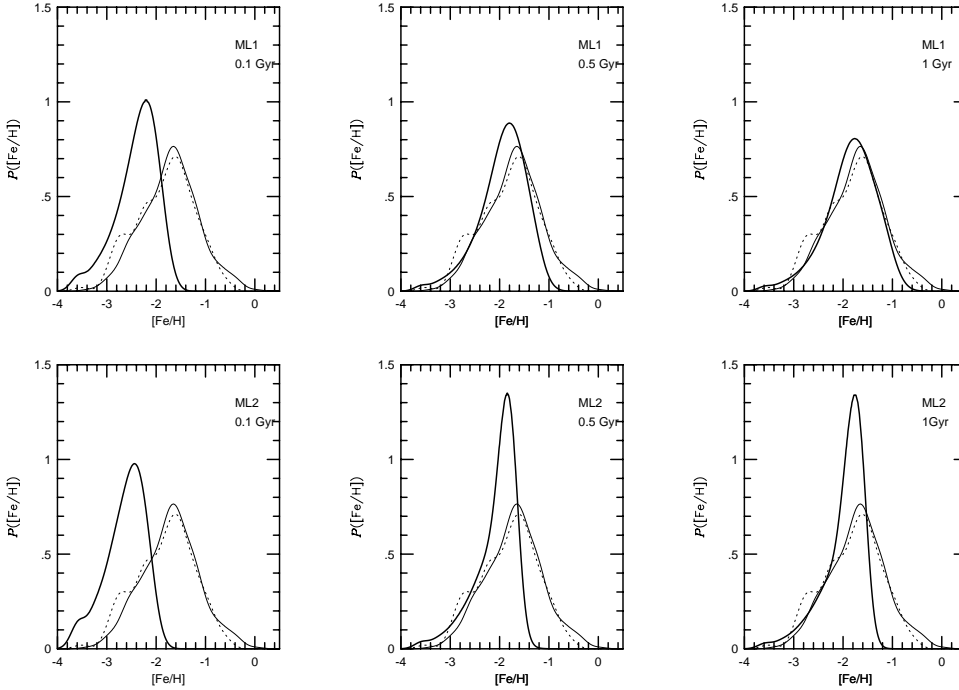


Fig. 9.. The GMDFs of model ML1 (upper three panels) and model ML2 (lower three panels) at 0.1, 0.5, and 1 Gyr. Thick solid lines show the theoretical GMDFs. Thin solid and dotted lines have the same meaning as in Fig. 6.

where $g(t)$, $c(t)$, and $Z_{\text{Sr}}(t)$ are the gas fraction, the SFR, and abundance of Sr in a block, respectively. The first and the second terms on the r.h.s. have the same meaning as those in equation (12). The third term comes from the delayed production, where p_i is the yield corresponding to the fixed time lag τ_i . Here $p_0 = 0.01$, $p_1 = 0.08$, $p_2 = 0.39$, $p_3 = 0.23$, $\tau_1 = 0.023$ Gyr, $\tau_2 = 0.025$ Gyr, and $\tau_3 = 2.7$ Gyr are assumed (PT97). The evolution of the iron abundance is calculated by equation (12).

The theoretical paths in figure 10 show that $[\text{Sr}/\text{Fe}]$ begins to increase rapidly at $[\text{Fe}/\text{H}] \sim -3.4$ in model S1 and $[\text{Fe}/\text{H}] \sim -2.3$ in model C, depending on the SFR. These paths roughly outline the dispersion of observed $[\text{Sr}/\text{Fe}]$ at $[\text{Fe}/\text{H}] \leq -2.5$. The models are calculated with a time step of 0.001 Gyr, which is shown by filled pentagons on the theoretical paths in figure 10. The chemical evolution from $[\text{Sr}/\text{Fe}] \sim -1.3$ to $[\text{Sr}/\text{Fe}] \sim 0$ should take place within a short time interval (~ 0.012 Gyr). After the rapid increase, the paths show temporal increase and decrease, and then converge. The declines of theoretical

$[\text{Sr}/\text{Fe}]$ are not because of delayed production of the iron (in other words, contribution from SNIa which produces the bulk of iron in the solar neighbourhood), since we assume that the time delay of iron τ in equation (12) is equal to 1.3 Gyr (see section 2.3) and consider chemical evolution before 1 Gyr. The declines of $[\text{Sr}/\text{Fe}]$ are due to onsets of the next formation of OB associations. Thus different SFR in each star forming region can explain the trends defined by a majority of observed stars on $[\text{Sr}/\text{Fe}]$ vs $[\text{Fe}/\text{H}]$ diagram.

Apparently the models are inconsistent with the observational data on figure 10. McWilliam et al (1995), Sneden et al (1996), and McWilliam (1998) have shown that the heavy element abundances in the super-solar $[\text{Sr}/\text{Fe}]$ stars are dominated by the r-process abundance patterns. The r-process elements can only be produced by Type II supernova events. Therefore one may argue that the time-delay model for Sr is inadequate to explain the observations. If the strontium is produced in all progenitors of SN II, however, $[\text{Sr}/\text{Fe}]$ values observed

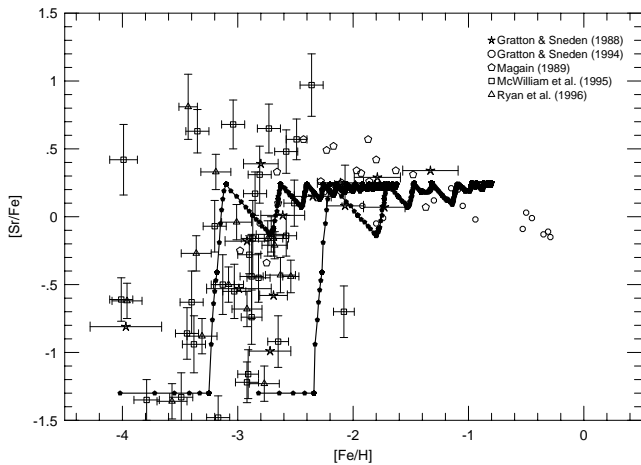


Fig. 10.. Chemical evolution of strontium. Observational data are taken from Gratton & Sneden (1988; 1994), Magain (1989), McWilliam et al. (1995), and Ryan et al. (1996). Two theoretical paths correspond to different SFR in a block. The left and right paths are obtained by adopting the same parameters as those of models S1 and C, respectively. Each filled pentagon on the paths indicates a time step 0.001 Gyr.

in metal-poor stars should be always super-solar. On the contrary, as we mentioned before, figure 10 shows that $[\text{Sr}/\text{Fe}]$ tends to decrease at lower iron abundance ($[\text{Fe}/\text{H}] \leq -2.5$). This drop suggests that the strontium was formed slightly later than the iron (see Mathews, Bazan, & Cowan 1992).

If the large scatter of $[\text{Sr}/\text{Fe}]$ observed for stars of iron abundance in the range of $-3.6 \leq [\text{Fe}/\text{H}] \leq -2.6$ is indeed due to a sharp increase of the Sr production rate, the Sr abundances of four extremely metal-deficient stars with $[\text{Fe}/\text{H}] \sim -4$ seem to show some evidence against it. However, the iron abundance measurement of such very low metal stars is extremely difficult and these iron abundances could well be as large as $[\text{Fe}/\text{H}] \gtrsim -3.6$ (M. Spite, private communications).

The theoretical $[\text{Sr}/\text{Fe}]$ is too low to fit to the observed extremely high $[\text{Sr}/\text{Fe}]$ value. However, the abundance of these stars might not reflect the composition of ISM from which they formed (e.g. McClure 1984). We should reject CH stars when we discuss the Galactic chemical evolution, because atmospheres of CH stars are thought to have been enriched by elements transferred from evolved companion AGB stars (McClure 1984). McWilliam et al (1995) and McWilliam (1998) reported that CS22898-027 ($[\text{Fe}/\text{H}] = -2.36$) and CS22947-187 ($[\text{Fe}/\text{H}] = -2.5$) are probably CH stars. Observational errors might also reflect the $[\text{Sr}/\text{Fe}]-[\text{Fe}/\text{H}]$ diagram. For a star CS22891-

209 ($[\text{Fe}/\text{H}] \sim -3.2$), Primas, Molaro, & Castelli (1994) and McWilliam et al (1995) reported $[\text{Sr}/\text{Fe}] = 0.92$ and $[\text{Sr}/\text{Fe}] = -0.07$, respectively, although they used the same lines and had the same S/N.

6. Conclusion

A stochastic chemical evolution model has been built to study an early history of metal enrichment in the Galactic halo. The metallicity distribution function of long-lived halo stars is found to be a clue to obtain the best model prescriptions. We find that the star formation in the halo virtually terminated by ~ 1 Gyr and that the halo has never been chemically homogeneous in its star formation history. The star formation in the halo could either be spontaneous or stimulated, which keep the halo always inhomogeneous and the turbulent mixing is found to be inefficient. This conclusion does not depend whether the mass loss from the halo is taken into account or not. The observed ratios of the α -elements with respect to the iron do not show scatters on the $[\alpha/\text{Fe}]-[\text{Fe}/\text{H}]$ plane, but this does not imply that the ISM in the halo was homogeneous because the chemical evolution path on this diagram is degenerate in the SFR. On the other hand, the apparent spread of $[\text{Sr}/\text{Fe}]$ ratio among metal-poor halo stars does not reflect an inhomogeneous metal enrichment, instead it is due to a sharp increase in the production rate of strontium that is probably synthesised in slightly less massive stars than the progenitor of iron-producing SN II.

We are grateful to an anonymous referee for a careful reading of the manuscript and for useful comments. C.I. thanks to the Japan Society for Promotion of Science for a financial support. This work was financially supported in part by a Grant-in-Aid for the Scientific Research (No. 0940311) by the Japanese Ministry of Education, Culture, Sports and Science.

References

- Allen D.A., Burton, M.G. 1993, *Nature* 363, 54
- Arimoto N., Matsushita, K., Ishimaru, Y., Ohashi, T., Renzini A. 1997, *ApJ* 477, 128
- Arimoto N., Yoshii, Y., Takahara, F. 1992, *A&A* 253, 21
- Audouze J., Silk J. 1995, *ApJ* 451, L49
- Bahcall J.N., Pinsonneault M.H. 1996, *AAS* 189, 5601
- Bateman N.P.T., Larson R. 1993, *ApJ* 407, 634
- Barbuy B. 1988, *A&A* 191, 121
- Beers T.C., Preston G.W., Shectman S.A. 1992, *AJ* 103, 1987
- Blaauw A. 1964, *ARA&A* 2, 213
- Bruhweiler F.C., Gull, T., Kafatos M., Sofia S. 1980, *ApJ* 238, L27

- Cash W., Charles P., Bowyer S., Walter F., Garmire G., Riegler G. 1980, *ApJ* 238, L71
- Carraro G., Chiosi C. 1994, *A&A* 281, 35
- Carney S.G., Laird J.B., Latham D.W., Aguilar L.A. 1996, *A&A* 112, 668
- Cioffi D.F., McKee C.F., Bertschinger E. 1988, *ApJ* 334, 252
- Copi C.J. 1997, *ApJ* 487, 704
- Cox D. P. 1972, *ApJ* 178, 159
- Edvardsson B., Andersen J., Gustafsson B., Lmbert D.L., Tomkin J. 1993, *A&A* 275, 101
- Elmegreen B.G. 1982, in *Submillimeter Wave Astronomy*, ed. J.E. Beckman, J.P. Phillips (Cambridge University Press) p5
- . 1985a, in *Birth and Infancy of Stars*, ed. R. Lucas, A. Omont, R. Stora (Amsterdam: Elsevier) p215
- . 1985b, in *Brith and Evolution of Massive Stars and Stellar Collapse*, ed W. Boland, H. van Woerden (Dordrecht: Reidel) p227
- Elmegreen B.G., Lada, C.J. 1977, *ApJ* 214, 725
- Fich M., Tremaine, S. 1991, *ARA&A* 29, 409
- Gratton R.G., Sneden C. 1988, *A&A* 204, 193
- Gratton R.G., Sneden C. 1994, *A&A* 287, 927
- Hartwick, F.D.A., 1976, *ApJ* 209, 418
- Henning T., Gürlér J. 1986, *Ap&SS* 128, 199
- Heiles C. 1987, *ApJ* 315, 555
- van den Hoek L.B., de Jong T. 1997, *A&A* 318, 231
- Hoyle F., 1953, *ApJ* 118, 513
- Humphreys, R.M. 1978, *ApJS*, 38, 309
- Lada C.J., Blitz L., Elmegreen B. 1979, in *Protostars and Planets*, ed T. Gehrels (Tucson: University of Arizona Press) p368
- Laird J.B., Rupen M.P., Carney B.W., Latham D.W. 1988, *AJ* 96, 1908
- Larson R.B. 1974 *MNRAS*, 169, 229
- Mac Low M.-M., McCray R. 1988, *ApJ* 324, 776
- Magain P. 1989, *A&A* 209, 211
- Mathews, G.J., Bazan, G., Cowan, J.J. 1992, *ApJ* 391, 719
- McCray R., Kafatos M. 1987, 317, 190
- McClure R.D. 1984, *PASP*, 96, 117
- McWilliam A 1997, *ARA&A* 35, 503
- McWilliam A 1998, *AJ* 115, 1640
- McWilliam A., Preston G. W., Sneden C., Sheckman S. 1995, *AJ* 109, 2757
- Nissen P.E., Gustafsson B., Edvardsson B., Gilmore G. 1994, *A&A* 285, 440
- Pagel B.E.J., 1992, in *The Stellar Populations of Galaxies*, IAU Symposium No. 149, edited by B. Barbuy & Renzini (Kluwer, Dordrecht), p. 133
- Pagel B.E.J., Tautvaišienė G. 1995, *MNRAS* 276, 505 (PT95)
- Pagel B.E.J., Tautvaišienė G. 1997, *MNRAS* 288, 108 (PT97)
- Pilyugin L.S. 1996, *A&A* 313, 803
- Primas F., Molaro, P., Castelli, F. 1994, *A&A* 290, 885
- Roy J.-R., Kunth D. 1995, *A&A* 294, 432
- Ryan S.G., Norris J.E. 1991, *AJ* 101, 1865
- Ryan S.G., Norris J.E., Beers T.C. 1996, *ApJ* 471, 254
- Saito M. 1979, *PASJ* 31, 181
- Salpeter E.E. 1955, *ApJ* 121, 161
- Searle L., Zinn R. 1978, *ApJ* 225, 357
- Schmidt M 1959, *ApJ* 129, 243
- Seal L., Zinn R. 1978, *ApJ* 225, 357
- Silk J. 1977, *ApJ* 214, 718
- Shigeyama T., Nomoto K., Hashimoto M. 1988, *A&A* 196, 141
- Sneden, C., McWilliam, A., Preston, G.W., Cowan, J.J., Burris, D.I., Armosky, B.J., 1996, *ApJ* 467, 819
- Stuart A., Ord, J.K. 1987, in *Kendall's Advanced Theory of Statistics*, 5th ed. (London: Griffin and Co.)
- Tenorio-Tagle G., Bodenheimer P. 1988, *ARA&A* 26, 145
- Timmes F. X., Woosley S. E., Weaver T. A. 1995, *ApJS* 98, 617
- Tinsley B. M. 1980, *Fund. Cosmic Phys.* 5, 287
- Wielen R., Fuchs B., Dettbarn C. 1996, *A&A* 314, 438
- Wilmes M., Köppen J. 1995, *A&A* 294, 47